Nuclear Instruments and Methods in Physics Research A 829 (2016) 372–375

Contents lists available at ScienceDirect

Nuclear Instruments and Methods in Physics Research A

journal homepage: www.elsevier.com/locate/nima

Particle-In-Cell simulation of laser irradiated two-component microspheres in 2 and 3 dimensions

Viktoria Pauw [a,*], Tobias M. Ostermayr [a,b], Karl-Ulrich Bamberg [a,c], Patrick Böhl [a], Fabian Deutschmann [a], Daniel Kiefer [a], Constantin Klier [a], Nils Moschüring [a], Hartmut Ruhl [a]

[a] Ludwig-Maximilians-Universität München, 80539, Germany
[b] Max-Planck-Institut für Quantenoptik, 85748 Garching, Germany
[c] Leibniz-Rechenzentrum, 85748 Garching, Germany

ARTICLE INFO

Available online 12 February 2016

Keywords:
PIC
Ion acceleration
3D3V
Mass limited target
Multispecies target
Coulomb explosion

ABSTRACT

We examine proton acceleration from spherical carbon-hydrogen targets irradiated by a relativistic laser pulse. Particle-In-Cell (PIC) simulations are carried out in 2 and 3 dimensions (2D and 3D) to compare fast proton spectra. We find very different final kinetic energies in 2D and 3D simulations. We show that they are caused by the different Coulomb fields in 2D and 3D. We propose a correction scheme for the proton energies to test this hypothesis. In the case of sub-focus diameter targets comparison of corrected 2D energies with 3D results show good agreement. This demonstrates that caution is required when modeling experiments with simulations of reduced dimensionality.

1. Overview

1.1. Motivation

Recently many simulations and experiments have been carried out to investigate the properties of fast particles emitted from plasmas that are produced when mass limited targets are irradiated by relativistic pico- or femtosecond laser pulses (comp. [6,10,8,14,11]). The long-term goal of these investigation is to develop new accelerating technologies and radiation sources. The cooperative effort of experiment and simulation in this area is fruitful for both fields, as comparing the results can help to improve the methods and models used by both. The simulations presented here are carried out in the context off recent experiments using levitating targets by the group of Jörg Schreiber at LMU (Garching). We make use of the PSC [7,1,5,4] developed at the chair for Computational Physics at LMU to simulate the interaction of isolated spherical two-component targets with relativistic laser pulses lasting 55 fs. We ask whether a two dimensional representation can yield satisfying results by comparing these to 3D simulations.

1.2. Set-up

The target in the associated experiment is a polystyrene ball of varying diameter consisting of a 1:1 mixture of hydrogen and carbon. It is modeled by a spherical plasma (fully ionized ab initio) with the corresponding amount of electrons (1 per hydrogen, 6 per carbon ion). We scan the properties of the resulting proton spectrum for different target sizes, ranging in diameter from 500 nm to 20 μm.

A 55 fs FWHM Gaussian laser pulse ($\lambda = 1$ μm, 8.3 μm FHWM transversal Gaussian profile) is seeded into the simulation domain.

A rectangular simulation domains of 2048×4096 cells in 2D and $2688 \times 1536 \times 1536$ cells for 3D are used corresponding to a spatial resolution of 64 cells per micrometer. For 2D simulations, boundaries are open at the slice edges and periodic on the slice planes (y direction) for fields and particles. For 3D simulations all boundaries are open. To avoid the danger of unstable plasma wave modes due to the finite resolution (as described in [15]), we use one half of the solid density n_s of polystyrene corresponding to $n_s/2 = 1.7 \cdot 10^{23}/\mathrm{cm}^3$, unless otherwise specified. For the same reason particles of the target are initiated with a Maxwellian momentum distribution corresponding to a plasma temperature in the keV range. Unless specified otherwise the initial temperature was 10 keV in the simulations.

* Corresponding author.
E-mail address: viktoria.pauw@physik.uni-muenchen.de (V. Pauw).

http://dx.doi.org/10.1016/j.nima.2016.02.012
0168-9002/

2. 2 Dimensional simulations

Since the computational load (machine run time and data output) is much smaller in 2D as compared to 3D, a reduced dimension model is often employed (for example [2,8,3,11]). We try to investigate whether simulations with reduced dimensions can still lead to reliable results for the scenario of a short laser pulse interacting with polystyrene microspheres as described in this paper.

The 2D geometry implies that the linear polarized laser pulse interacts with a cylinder rather than a sphere. This means that the laser can be polarized either along the cylinder axis (s-polarization, 2D-s) or perpendicular to it (p-polarization, 2D-p). We expect that the s and p cases lead to different results for otherwise same parameters.

2.1. Difference between polarization directions

The electron motion is governed by the Lorentz force leading to ponderomotive potential effects. For p-polarization significant numbers of electrons can move along the electric field and be extracted from the target, forming ultrashort bunches separated by one laser wavelength (see Fig. 1). This process is described in detail in [9]. For the s-polarization case displacement along the direction of the electric field is impossible. However, electrons still experience the $\vec{j} \times \vec{B}$-force, but do not form bunches to the same extent as in the p case. Since the $\vec{j} \times \vec{B}$-force changes sign 4 times during a laser cycle, density modulations with the separation of half a wavelength are observed. In addition the longitudinal ponderomotive force is overestimated as electrons only see the maximum field strength in the middle of the pulse (see Fig. 1). We also note that for a 2 μm target average electron temperature is 0.3 MeV for p but only 0.12 MeV for s-polarization, in both cases exceeding the initial temperature substantially.

We observe that ion kinetic energies are significantly higher in the p case than in the s case. The energy mismatch is largest for the smallest targets as is seen in Fig. 2. We attribute this mismatch in energy to a difference in electron removal, which in the p case is about 77% for 0.5 μm and 12% for a 2 μm target, but much lower in the s case (40% for 0.5 μm and 3% for 2 μm). Here we specify the percentage of electrons still present in a 16×32 μm rectangle around the target 500 fs after pulse maximum. The suppressed electron depletion in the s-case obviously implies, that a 2D-s set-up cannot model the interaction scenarios in 3D.

The rising maximal energies for smaller target radii in the p-case do not agree with experimental findings (e.g. [13,12]). Noticeably the protons continue to considerably gain kinetic energy until they reach the simulation domain boundaries. This is caused by the Coulomb field of the positive charge surplus at the target. To retrieve reliable kinetic energy spectra we conduct 3 dimensional simulations of the same set-up.

3. 3 Dimensional simulations

The same set-up was then simulated in 3D using the same resolution and pulse parameters but a shorter box ($2688 \times 1536 \times 1536$ cells) to reduce memory demand.

When comparing the p-pol 2D set-up with a slice of the 3D simulation domain along the laser electric field polarization

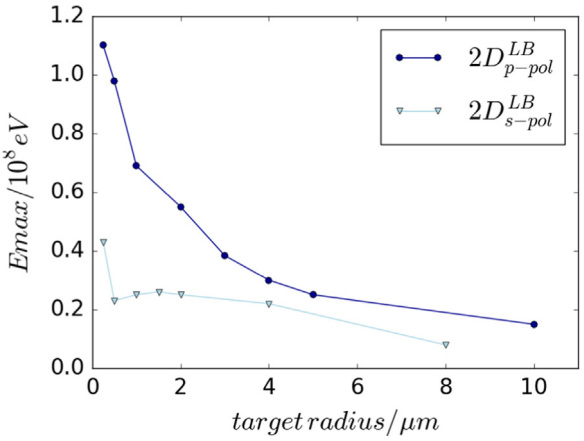

Fig. 2. Maximum proton energies for p and s polarized laser field using a long box (2048×4096, corresponding to 32 μm and 64 μm), an initial temperature of 50 keV, $n_0 = 0.25 \cdot n_s$ and $a_0 = 15$.

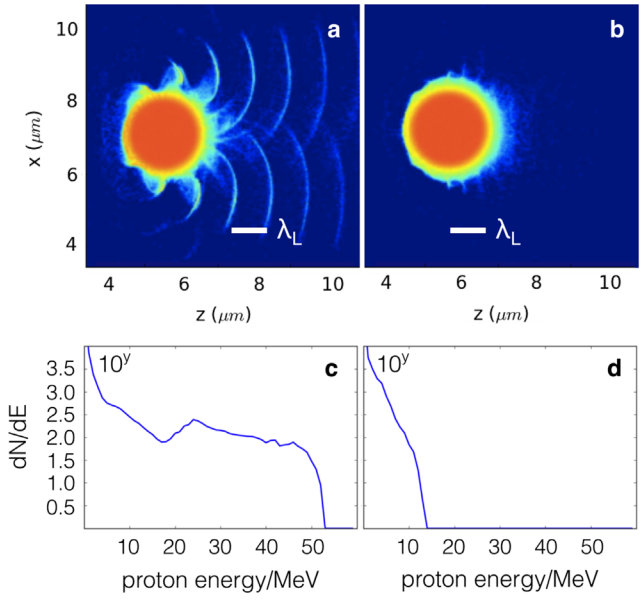

Fig. 1. 2D simulation of a 2 μm target, $a_0 = 12$, laser wavelength $\lambda = 1$ μm. Above: Qualitative comparison of electron dynamics in the p (a) and s (b) polarization case (electron density). We observe the different frequency of the density waves. Below: Proton energy spectrum 200 fs after pulse maximum (power of 10 of the number of quasi-particles, p-pol (c) and s-pol (d)).

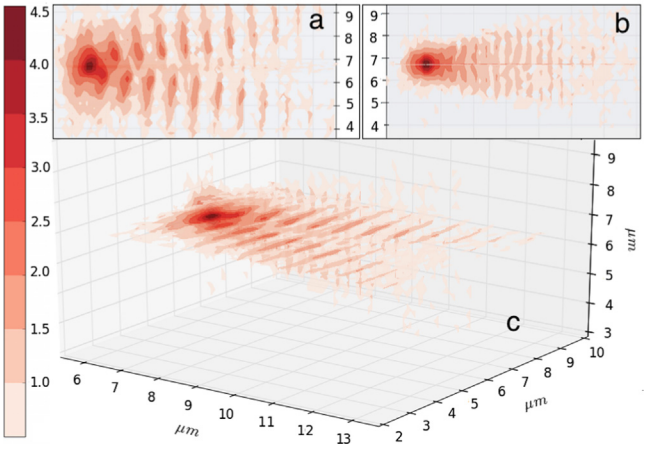

Fig. 3. 500 nm target in 3D, $a_0 = 12$. Contour plot of electron density in 50 nm slices through the center of the 3D simulation domain: (a) in polarization plane, (b) perpendicular to polarization plane and (c) both. The ultrashort electron bunches appear as in the 2D-p case. Density scale shows the powers of 10 of the number of quasi-particles in a slice volume element $10\Delta x \cdot 10\Delta x \cdot \Delta x$.

direction and comparing the s-pol case with a slice perpendicular to the E-field, the qualitative particle motion is the same.

We find that many features of the proton spectra from the 3D simulations agree with the 2D-p simulations, while the achieved proton energies lie close to the ones obtained in 2D-s (comp. Fig. 5). This is peculiar as the charge removal by the ultrashort electron bunches in 2D-p is also observed in 3D and 2D-p should in principle produce energies closer to the 3D results. The reason why this is not the case is discussed in the following section.

As can be seen from Fig. 4 that there is a distinctive difference in the proton spectrum for targets 0.5 μm and those with a larger diameter. The 500 nm diameter target shows a non-monotonic spectrum. For this target all protons are pushed out of the carbon region and we have features of a Coulomb explosion regime. For larger targets the acceleration appears to be predominantly driven by surface effects.

4. Comparison between 2D and 3D results

Comparison of the 2D and 3D results shows that particle motion can be described in the reduced dimension set-up. The 2D-p scenario shows the characteristic dynamics of a 3D domain slice in E-field direction and the slice perpendicular to the E-field having the same qualitative particle distribution of the 2D-s simulation (comp. Fig. 3). The 3D target shows a similar percentage of charge removal as in the 2D-p case. But the kinetic energies acquired by the ions are very different. These differences can be attributed mostly to the Coulomb field in the 2D geometry that is not the same as in the 3D case. In 2D the target set-up represents an infinite cylinder. When a charge separation occurs in the simulation volume an infinite line charge is effectively created in 2D. Such a charge causes a field of the form

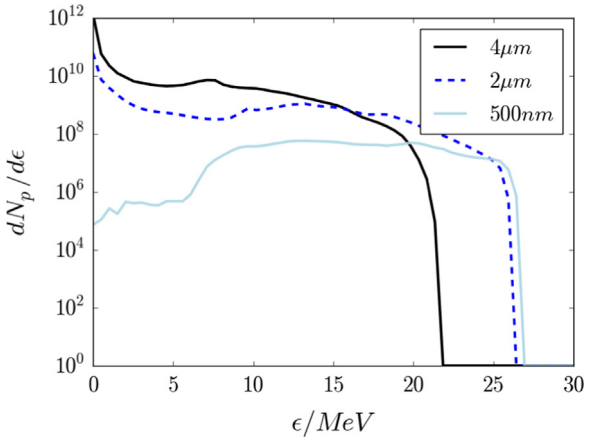

Fig. 4. Proton spectrum for different target diameters, $a_0 = 12$ μm.

$$E_{2D}(r) = \frac{\lambda_0}{2\pi\epsilon_0 r} = \frac{\rho_0 R^2}{2\epsilon_0 r} \tag{1}$$

with the line charge

$$\lambda_0 = \frac{Q}{\Delta x} = \rho_0 \pi R^2, \tag{2}$$

were R is the target radius, and $r > R$ the distance of the probe charge from the target center. This field is different from the 3D Coulomb field of a sphere, that declines as r^{-2}. This explains the different results for 2D and 3D simulations as well as the fact that a longer detection distance relative to the target size produces higher energies, because the particles experience a more extended accelerating field in 2D. For a simple analysis we model the proton acceleration by a Coulomb repulsion by a spherical/cylindrical positive charge surplus at the target location. For a quantitative analysis we assume that the 2D and 3D simulation set-ups are capable of generating the same positive charge density in our spheres. Based on this assumption we obtain the corresponding 2D line charge and the Coulomb fields in 2D and 3D. Then we calculate the energy gain of the protons related to the Coulomb fields of the protons in 2D and 3D. For a the sake of simplicity we assume rotational symmetry and a homogenous line charge $\lambda_0 = \frac{Q}{\Delta x}$ which corresponds to a homogenous volume charge $\rho_0 = \frac{Q}{\Delta V} \rightarrow \lambda_0 = \pi R^2 \rho_0$.

For a probe particle that starts at the surface point R of the carbon population with zero kinetic energy and is detected at the position r^e we find

$$\varepsilon_{det}^{2D} = \frac{\lambda_0}{2\pi\epsilon_0} \ln\frac{r_e}{R}, \tag{3}$$

$$\varepsilon_{det}^{3D}(R) = \frac{\rho_0 R^3}{3\epsilon_0}\left(\frac{1}{R} - \frac{1}{r_e}\right). \tag{4}$$

We assume that R corresponds to the boundary of the carbon region. Equating the maximum energy attainable by the Coulomb field of a sphere and a cylinder of Radius R we obtain:

$$\varepsilon_{det}^{3D}(R) = \frac{\rho_0 R^3}{3\epsilon_0}\left(\frac{1}{R} - \frac{1}{r_e}\right) = \frac{\lambda_0}{3\epsilon_0 \pi}\left(1 - \frac{R}{r_e}\right) = \frac{2}{3}\frac{\varepsilon_{det}^{2D}}{\ln(\frac{r_e}{R})}\left(1 - \frac{R}{r_e}\right) \tag{5}$$

We recalculate the ion spectrum with this model using position and momentum information for each quasi-particle at a time where laser interaction is over about 200 fs after the pulse maximum but all protons are still in the simulation domain.

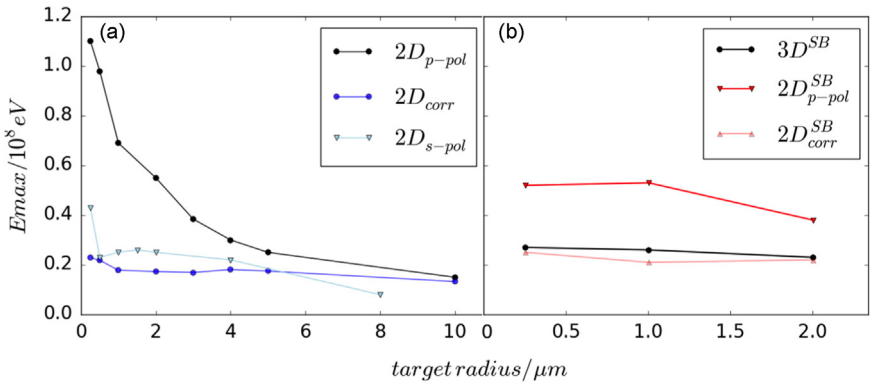

Fig. 5. Comparison of maximum proton energies: (a) 2D simulation in the long box set-up (2D); s- and p-pol and corrected p-pol data. (b) 2D and 3D simulations in small-box set-up.

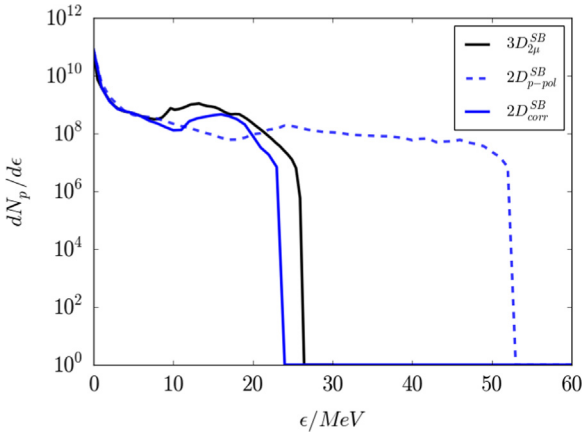

Fig. 6. Proton spectrum of the 2 μm target in 3D, 2D and corrected 2D according to algorithm (5). $a_0 = 12$, 2D particle numbers are re-normalized to match particle numbers in 3D by $\frac{N_{3D}}{N_{2D}} = \frac{4}{3}\frac{R}{\Delta x}$ to make the difference in spectra more visible.

We obtain the distance from the target surface r_e and calculate the ratio with radius of the carbon sphere R. If $\ln(\frac{r_e}{R}) > 1$, we then obtain the corresponding ε^{3D} according to Eq. (5). The resulting spectrum and maximal energy can then be compared with the one obtained in a full 3D simulation to see whether the spectrum is alike and similar energies are obtained. In spite of the starkly simplified model employed this is indeed the case for the 0.5, 2 and 4 μm targets (comp. Figs. 5 and 6).

Fig. 6 shows that corrected 2D-p proton spectra of the 2 μm match the 3D results. Proton energies (but not necessarily $\frac{dN}{d\epsilon}$) can be approximated by running 2D-p simulations and taking the Coulomb correction into account. We note that our approach only applies where a pure Coulomb field dominates proton acceleration. We expect that this is the case for small, mass limited targets since the laser driver must be able to remove large numbers of electrons from the target.

However we do not capture differences in the dynamics inside the dense region around the target as the algorithm only applies to particles that are already at a distance of $r_e > e_N \cdot R$ from the carbon surface (e_N denotes Euler's number). It is assumed that the particle has a low velocity at the target surface R. Also the model neglects other differences between 2D and 3D geometry such as surface to volume ratio and cannot be expected to be valid for all parameter ranges and set-ups. Therefore we cannot produce reliable results by simply applying such a method. A 3D simulation must be used to obtain physically correct spectra. For small targets that are completely in the Coulomb Explosion regime, a more refined model could be developed, that may reliably produce correct results.

5. Conclusion

We have investigated the interaction of microspheres with $R = 0.5, 2, 4$ μm with short laser pulses at $a_0 = 12$ in 2D-s, 2D-p, and 3D. We find that both, 2D-s and 2D-p set-ups show features present in 3D. Slices taken through the center of the spheres perpendicular to the electric field in the 3D setup show features that resemble those of the 2D-s simulations. Slices through the center of the spheres along the electric field direction in 3D show features that resemble those of 2D-p simulations. We find that the energy spectra of the protons in 3D can be approximated with the help of simulations with 2D-p setup and the Coulomb correction. The fact that 2D-s and 3D proton spectra seem to agree in our simulations is by pure chance since a 2D-s setup is not capable of modeling the physics correctly. It is rather the combination of enhanced Coulomb fields and reduced charge removal in 2D-s that yield similar proton energies in our simulations as one effect cancels the error of the other. This conclusion is not restricted to the spherical targets investigated in our paper.

Acknowledgments

The PSC is developed by Hartmut Ruhl and colleagues at the chair for Computational and Plasma Physics (LMU). 3D simulations were carried out on the SuperMUC Phase-2 at LRZ in Garching. Computer resources for this project have been provided by the Gauss Centre for Supercomputing/Leibniz Supercomputing Centre under grant: pr84me. The authors acknowledge helpful discussions with J. Schreiber. Financial support came from IMPRS-APS (K.-U. B. and T.M.O.) and the IFE Keep-in-Touch acitivity within the Eurofusion consortium (Project No. ToIFE 2015-2017) (T.M.O.). The PSC project is partially funded by Deutsche Forschungsgemeinschaft under contract EXC-158 (cluster of excellence MAP). This work has been carried out within the framework of the EUROfusion Consortium and has received funding from the Euratom research and training programme 2014-2018 under grant agreement No 633053. The views and opinions expressed herein do not necessarily reflect those of the European Commission.

References

[1] ⟨http://fishercat.sr.unh.edu/psc/index.html⟩. ⟨http://www.plasma-simulation-code.net/people/index.html⟩, 2013.
[2] A.J. Kemp, H. Ruhl, Physics of Plasmas 12 (2005).
[3] A.A. Andreev, J. Limpouch, J. Psikal, K. Yu Platonov, V.T. Tikhonchuk, The European Physical Journal Special Topics 175 (2009).
[4] K. Bamberg, F. Deutschmann, N. Moschuering, H. Ruhl, inSIDE 13 (2) (2015) 22ff.
[5] K. Bamberg, H. Ruhl, inSIDE 12 (2) (2014) 51ff.
[6] H. Daido, M. Nishiuchi, S. Pirozhkov, Reports on Progress in Physics 75 (056401) (2011).
[7] K. Germaschewski, W. Fox, N. Ahmadi, L. Wang, H. Ruhl, A. Bhattacharjee, The plasma simulation code: a modern particle-in-cell code with load-balancing and GPU support ⟨www.sciencedirect.com⟩, 2013.
[8] J. Limpouch, J. Psikal, V.T. Tikhonchuk, O. Klimo, A.V. Brantov, A.A. Andreev, Journal of Physics: Conference Series 112 (2008).
[9] T.V. Liseykina, S. Pirner, D. Bauer, Physical Review Letters 104 (095002) (2010).
[10] A. Macchi, M. Borghesi, M. Passoni, Review of Modern Physics 85 (2013).
[11] S. Buffechoux, J. Psikal, M. Nakatsutsumi, Physical Review Letters 105 (015005) (2010).
[12] S. Ter-Avetisyan, B. Ramakrishna, et al., Physics of Plasmas 19 (145006) (2012).
[13] S. Ter-Avetisyan, M. Schnürer, P.V. Nickles, V. Tikhonchuk, et al., Physical Review Letters 96 (073112) (2006).
[14] T. Kluge, W. Enghardt, S.D. Kraft, Physics of Plasmas 17 (123103) (2010).
[15] D. Tskhakaya, K. Matyash, R. Schneider, F. Taccogna, Contributions to Plasma Physics 47 (8–9) (2002).